HOKKAIDO UNIVERSITY

| | |
|---|---|
| Title | Redox characteristics variations in the cation-ordered perovskite oxides BaLnMn(2)O(5+delta) (Ln = Y, Gd, Nd, and La) and Ca2Al1-xGaxMnO5+delta (0 <= x <= 1) |
| Author(s) | Motohashi, Teruki; Kimura, Makoto; Inayoshi, Takeru; Ueda, Taku; Masubuchi, Yuji; Kikkawa, Shinichi |
| Citation | Dalton transactions, 44(23), 10746-10752<br>https://doi.org/10.1039/c4dt03863k |
| Issue Date | 2015 |
| Doc URL | http://hdl.handle.net/2115/62253 |
| Type | article (author version) |
| File Information | Motohashi.pdf |

Instructions for use

Hokkaido University Collection of Scholarly and Academic Papers : HUSCAP

*Dalton Transactions*, 2015, **44**, 10746-10752.

# Redox characteristics variations in the cation-ordered perovskite oxides Ba*Ln*$Mn_2O_{5+\delta}$ (*Ln* = Y, Gd, Nd, and La) and $Ca_2Al_{1-x}Ga_xMnO_{5+\delta}$ ($0 \leq x \leq 1$)

Teruki Motohashi,* Makoto Kimura, Takeru Inayoshi, Taku Ueda, Yuji Masubuchi, and Shinichi Kikkawa

Two series of manganese-based oxygen storage materials, Ba*Ln*$Mn_2O_{5+\delta}$ (*Ln* = Y, Gd, Nd, and La) and $Ca_2Al_{1-x}Ga_xMnO_{5+\delta}$ ($0 \leq x \leq 1$), were synthesized and characterized to clarify cationic substitution effects on the oxygen intake/release behaviors of these materials. The thermogravimetric data revealed that the isovalent substitutions neighboring the active sites for oxygen intake/release are very effective. For Ba*Ln*$Mn_2O_{5+\delta}$, fully-reduced $\delta \approx 0$ products with larger *Ln* ions showed oxygen intake starting at lower temperatures in flowing $O_2$ gas, resulting in a systematic relation between the onset temperature and ionic radius of $Ln^{3+}$. Furthermore, the $\delta$ vs $P(O_2)$ plots at 700 °C indicated a systematic trend: the larger the ionic size of $Ln^{3+}$ is, the larger oxygen contents the *Ln*-products exhibit. For $Ca_2Al_{1-x}Ga_xMnO_{5+\delta}$, on the other hand, the temperature-induced oxygen intake/release characteristics appeared to be influenced by Ga-for-Al substitution, where the onset temperatures of oxygen release (upon heating) and oxygen intake (upon cooling) are decreased with increasing the Ga content (*x*).

*Faculty of Engineering, Hokkaido University, N13, W8, Kita-ku, Sapporo Hokkaido 060-8628, Japan.*

*Corresponding Author. Faculty of Engineering, Hokkaido University, N13, W8, Kita-ku, Sapporo Hokkaido 060-8628, Japan. E-mail: t-mot@eng.hokudai.ac.jp; Tel: +81-(0)11-706-6741; Fax: +81-(0)11-706-6740.

†Electronic supplementary information (ESI) available. See DOI: 10.1039/XXXXXX.

## 1. Introduction

Driven by critical issues such as the depletion of petroleum resources and global warming, environmental protection and energy conservation have represented the major scientific challenges. Since oxygen is the most ubiquitous element that is responsible for a huge variety of chemical reactions in manufacturing industries and energy productions, oxides with significant redox activities have attracted increased attention. The “oxygen storage materials (= OSMs)”, which are featured with rapid and reversible oxygen intake/release capability, are indeed within this class. The best-known OSM is $CeO_2$-$ZrO_2$ solid solution, the so-called CZ, has been applied to modern three-way catalysts of automobiles owing to its remarkable reactivity with three exhaust components, $NO_x$, CO, and hydrocarbons.[1] While CZ and its related materials (both of which contain cerium as a redox species) have been intensively studied, [1-4] an essentially different class of OSMs is also noteworthy when considering new oxygen-related applications.

As alternative high-performance OSMs, transition-metal oxides are worthy of attention because of flexible valence states of constituent transition metals. We recently reported the remarkable oxygen intake/release capability of two manganese oxides $BaYMn_2O_{5+\delta}$[5] and $Ca_2AlMnO_{5+\delta}$.[6] $BaYMn_2O_{5+\delta}$ is categorized as an *A*-site ordered double-perovskite which contains smaller yttrium and larger barium ions in alternate layers,[7-9] as illustrated in Fig. 1. The oxygen sites within the yttrium layer is readily filled/unfilled depending on temperature and/or the surrounding atmosphere, resulting in large oxygen nonstoichiometry ranging $0 \leq \delta \leq 1$. This oxide can rapidly store/release

a large amount of oxygen (> 3.7 wt%) at 500 °C upon switching the atmosphere between $O_2$ and 5% $H_2$/95% Ar in a perfectly reversible manner.[5] $BaYMn_2O_{5+\delta}$ may be used as reducing catalysts and oxygen getter, owing to its great affinity to oxygen.

$Ca_2AlMnO_{5+\delta}$ crystallizes in a Brownmillerite-type structure with a general formula of $A_2B_2O_5$, which consists of alternate stacking of tetragonal $BO_4$ and octahedral $BO_6$ layers with a preferential formation of $AlO_4$ and $MnO_6$ polyhedra,[11-13] as illustrated in Fig. 1. Our TG analysis revealed[6] that this oxide stores oxygen topotactically at low temperatures ($T$ < 600 °C) to transform into an oxygen-excess form, and releases the whole amount of excess oxygen at elevated temperatures ($T$ > 650 °C). This oxide is featured with significant oxygen intake/release capability even with small temperature variations, which may be applied to oxygen-related technologies involving a facile oxygen release process, such as oxygen-gas production/enrichment and cathode materials in SOFC.

It should be emphasized that $BaYMn_2O_{5+\delta}$ and $Ca_2AlMnO_{5+\delta}$ are categorized as nonstoichiometric oxides with perovskite-derived structures which facilitate cationic substitutions resulting from a flexible perovskite framework. For $BaYMn_2O_{5+\delta}$, substitutions of the lanthanoid (*Ln*) series at the yttrium site were extensively investigated, although the interests in previous works were mainly devoted to the electronic properties.[14-18] Recent reports by Swierczek and coworkers evidenced[19-21] that *Ln*-substituted derivatives of $BaYMn_2O_{5+\delta}$ also showed remarkable oxygen intake/release capability. It appeared that the operating temperature and reaction kinetics are more or less influenced by *Ln*-substitution, but the relation was unclear between the

constituent *Ln* species and characteristics. For $Ca_2AlMnO_{5+\delta}$, on the other hand, isovalent Sr-for-Ca and Ga-for-Al substitutions were previously examined by Antipov and coworkers.[22-25] They focused only on the crystal chemistry of the $(Ca,Sr)_2(Al,Ga)MnO_{5+\delta}$ family, and never studied details in the oxygen intake/release characteristics.

To accelerate the applied research on our OSMs for realizing the aforementioned oxygen-related applications, it is important to understand how the oxygen intake/release behaviors are influenced by cationic substitutions, especially for the constituent cations neighboring the active sites of oxygen intake/release. In the present work, the series of $BaLnMn_2O_{5+\delta}$ (*Ln* = Y, Gd, Nd, and La) and $Ca_2Al_{1-x}Ga_xMnO_{5+\delta}$ ($0 \leq x \leq 1$) were synthesized and characterized to clarify isovalent substitution effects on the oxygen intake/release behaviors. Our thermogravimetric data have indicated that the isovalent substitutions neighboring the active oxygen, that is, lanthanoids (*Ln*) for yttrium and gallium for aluminum, are indeed effective to control the redox characteristics of $BaYMn_2O_{5+\delta}$ and $Ca_2AlMnO_{5+\delta}$, even though the redox species (= manganese) has remained untouched for the both oxides.

## 2. Experimental section

### 2.1. Synthesis

Samples of $BaLnMn_2O_{5+\delta}$ (*Ln* = Y, Gd, Nd, and La) were synthesized via a citrate precursor route combined with the oxygen-pressure-controlled encapsulation

technique.[5,9] $Ln_2O_3$ (*Ln* = Y, Gd, and Nd, 99.9%, Wako Pure Chemical; *Ln* = La, 99.99%, Kanto Chemical; fired at 1000 °C overnight prior to use), $Ba(NO_3)_2$ (99.9%, Wako Pure Chemical), and $Mn(NO_3)_2 \cdot 6H_2O$ (99.9%, Wako Pure Chemical) were used as starting materials. Appropriate amounts of these reagents were dissolved in diluted $HNO_3$ (for $Ln_2O_3$) or Milli-Q water [for $Ba(NO_3)_2$ and $Mn(NO_3)_2 \cdot 6H_2O$] to prepare *Ln*, Ba, and Mn nitrate solutions. These solutions were mixed in a crucible in which equimolar citric acid (98%, Wako Pure Chemical) was subsequently added as a complexing agent. The citrate solution was stirred and heated at 60 ~ 70 °C to promote polymerization. The gelatinous product was prefired at 450 °C in air for 1 h and then at 1000 °C in flowing $N_2$ gas for 24 h. The resultant precursor powder was pressed into pellets and placed in an evacuated silica ampule together with an equiamount of FeO powder, which acts as a getter for excess oxygen. The silica ampule was heated at 1100 °C for 24 h, followed by quenching into ice water.

Samples of $Ca_2Al_{1-x}Ga_xMnO_{5+\delta}$ with $x$ = 0, 0.1, 0.3, 0.5, and 1.0 were synthesized via a citrate precursor route. Similarly to the above $BaLnMn_2O_{5+\delta}$, a gelatinous product was prepared starting from $(Ca(NO_3)_2 \cdot 4H_2O$ (99.9%, Kanto Chemical), $Al(NO_3)_3 \cdot 9H_2O$ (99.9%, Wako Pure Chemicals), $Ga(NO_3)_2 \cdot yH_2O$ (99.9%, Kojundo Chemical Laboratory, $y$ = 8.16 as determined by pyrolysis analysis), $Mn(NO_3)_2 \cdot 6H_2O$ and citric acid. The gelatinous product was calcined in air at 450 °C for 1 h, ground, pelletized, and then fired in air at 1000 °C for 12 h. The resultant pellet was again ground and pelletized, followed by firing at 1000°C for 10 h under reduced pressure (~ $10^{-1}$ Pa) to minimize the amount of excess oxygen in the $Ca_2Al_{1-x}Ga_xMnO_{5+\delta}$ phase.

### 2.2. Characterization

Phase purity was checked for the resultant products by means of X-ray powder diffraction (XRD; Rigaku Ultima IV; Cu Kα radiation). The lattice parameters for Ba*Ln*$Mn_2O_{5+\delta}$ and $Ca_2Al_{1-x}Ga_xMnO_{5+\delta}$ were determined on the basis of model-independent profile fits to the diffraction patterns utilizing Jana2006 software.[26] Oxygen contents (5+δ) of the products were precisely determined by iodometric titration. Details in the titration experiment are given elsewhere.[9] The grain morphology of each product was observed with scanning electron microscopy (SEM; JEOL JSM-6300F and JSM-6500F).

The oxygen intake/release characteristics of the products were investigated by means of thermogravimetry (TG; Rigaku TG8120). The measurements were carried out for 30 ~ 40 mg specimens of Ba*Ln*$Mn_2O_{5+\delta}$ and $Ca_2Al_{1-x}Ga_xMnO_{5+\delta}$ under various atmospheres. The composition of the flowing gas was controlled utilizing mass flow controllers and/or commercial gas mixtures. The detailed condition of each experiment is given in the next section.

## 3. Results

### 3.1. Ba*Ln*$Mn_2O_{5+\delta}$

The XRD data indicate that all the as-synthesized Ba*Ln*$Mn_2O_{5+\delta}$ products are essentially phase-pure of the fully reduced $\delta \approx 0$ form with a tetragonal unit cell, as presented in Fig. S1 of the ESI. The lattice parameters for the products are summarized in Table 1. Both of the *a*- and *c*-axis lengths are in agreement with those in the previous

literature.[8,9,15,16] As expected, these values systematically increase with increasing the ionic radius of $Ln^{3+}$ in the order of Y, Gd, Nd, and La.[27] The oxygen content (5+δ) values determined by iodometry are close to 5.00 for all the *Ln*-products (Table 1).

The oxygen intake behavior of $BaLnMn_2O_{5+\delta}$ was studied employing a temperature-programmed oxidation (TPO) method. In this experiment, the weight of the as-synthesized product was monitored by a thermobalance upon heating in flowing $O_2$ gas with a heating rate of 1 °C/min. As shown in Fig. 2, all the *Ln*-products exhibit a large weight gain most likely attributed to the increase in the oxygen content. The magnitude of the weight gain agrees well with the value expected for the $O_5$-to-$O_6$ transformation (a smaller weight gain for *Ln* = Gd, Nd, and La are simply due to their larger molar weights). For *Ln* = Y, the sample weight starts to increase at about 250 °C and then tends to be saturated above 370 °C, consistent with our previous report.[5] Noticeably, the Gd, Nd, and La-products show oxygen intake starting at lower temperatures, resulting in a systematic relation between the onset temperature and ionic radius of $Ln^{3+}$, as summarized in Table 1.

Since the oxygen intake/release processes involve redox reactions at the powder surface and ionic diffusion in crystallites, the oxygen intake/release kinetics should depend greatly on the grain size.[28] As demonstrated in Fig. S2 of the ESI, all of the *Ln*-products consist of coarse particles with a similar size of 1 ~ 2 μm, although the grain shape in the La-product is somewhat different from the other products. It is thus concluded that the influence of the grain morphology is negligible on the oxygen-intake onset temperature, and hence the systematic trend is a consequence of the intrinsic

redox property of the Ba*Ln*$Mn_2O_{5+\delta}$ series.

Next, isothermal TG experiments were performed under varying oxygen partial pressures ($P(O_2)$) to gain additional insights into the redox characteristics of the Ba*Ln*$Mn_2O_{5+\delta}$ series. The as-synthesized product was post-annealed at 500 °C in flowing $O_2$ gas, and then the weight of the product was monitored at 700 °C, while $P(O_2)$ was decreased in a stepwise manner from $10^5$ to 10 Pa. The magnitude of δ was calculated under the assumption that the $O_2$-annealed products are fully oxygenated with the highest oxygen content δ = 1, which was confirmed by iodometry. For the Y-product, the sample weight is immediately varied and then saturated when $P(O_2)$ is decreased, as presented in Fig. 3(a). Significantly, the oxygen content 5+δ gradually decreases in a pressure range of $10^5 \sim 3 \times 10^2$ Pa, and then exhibits an abrupt drop between δ ≈ 0.90 and 0.55 at $P(O_2) = 10^2$ Pa. The abrupt drop appears also in the isothermal TG data at 650, 750, 800, and 850 °C, which have been presented elsewhere.[29] This result clearly indicates the coexistence of two distinct phases with oxygenated δ ≈ 1 and intermediate δ ≈ 0.5 compositions in this oxide system. The intermediate δ ≈ 0.5 phase is known to crystallize in an orthorhombic structure which contains oxygen-vacancy ordering within the yttrium layer.[9,30]

Meanwhile, the oxygen release behaviors are clearly different for *Ln* = Gd, Nd, and La. As demonstrated by a representative TG curve in Fig. 3(b), the weight change upon lowering $P(O_2)$ is marginal for the Nd-product without abrupt drops. The magnitude of the oxygen-content variation Δδ is only 0.03 between $P(O_2) = 10^5$ and 10 Pa, being much smaller than Δδ = 0.48 for *Ln* = Y. It also appeared that the oxygen content of the

La-product is essentially constant in this $P(O_2)$ range. The resultant plots of the saturated δ vs $P(O_2)$ are summarized in Fig. 4. The plots indicate a systematic trend for Ba*Ln*$Mn_2O_{5+\delta}$: that is, the larger the ionic size of $Ln^{3+}$ is, the larger oxygen contents the *Ln*-products exhibit. While larger *Ln*-products remain in their oxygenated forms even in diluted oxygen atmospheres down to $P(O_2)$ = 10 Pa, the smallest *Ln* = Y undergoes a phase transformation to the partially reduced form. This implies that the oxidation (reduction) is easier for Ba*Ln*$Mn_2O_{5+\delta}$ with larger (smaller) $Ln^{3+}$ ions, consistent with the aforementioned TPO experiment (Fig. 2).

### 3.2. $Ca_2Al_{1-x}Ga_xMnO_{5+\delta}$

Single-phase $Ca_2Al_{1-x}Ga_xMnO_{5+\delta}$ products were successfully prepared for the whole Ga contents $x = 0 \sim 1$. The diffraction patterns are essentially similar for all the products and assignable to an orthorhombic Brownmillerite-type structure,[6,11-13] see Fig. S3 of the ESI. The lattice-parameter variations through Ga-for-Al substitution are obviously anisotropic. While the *a*- and *c*-axis lengths weakly depend on the Ga-content (*x*), the *b*-axis length along the stacking direction is enlarged markedly and linearly with increasing *x*, as shown in Table 2 and Fig. S4 of the ESI. This feature suggests that the structural change upon Ga substitution is mainly attributed to the increased thickness of the $(Al,Ga)O_4$ layer. The iodometric analysis revealed that all the products are close to oxygen stoichiometry but some contain small amounts of excess oxygen (Table 2), which would originate from stacking defects with respect to the ideal $(Al,Ga)O_4$-$MnO_6$ alternate sequence.

Isothermal TG experiments were performed on the $Ca_2Al_{1-x}Ga_xMnO_{5+\delta}$ products. The

sample weight was measured at 400 °C, while the flowing gas was switched from $N_2$ ($P(O_2) \approx 1$ Pa) to $O_2$ to monitor the oxygen intake process. For $x = 0 \sim 0.5$, the excess oxygen amount (estimated from the weight gain) rapidly increases under $O_2$ atmosphere, and then tends to be saturated at $\delta = 0.40 \sim 0.45$, as shown in Fig. 5. The slightly smaller values than the maximum oxygen content ($\delta = 0.50$) imply that the $O_5$-to-$O_{5.5}$ transformation is not ideal. Noticeably, the oxygen intake rate is significantly slower for $x = 1$ than $x = 0 \sim 0.5$. Taking into account the fact that the grain morphology (SEM; see Fig. S5 of the ESI) is rather similar for all the products, the slower oxygen intake of the $x = 1$ product could be attributed to the lowered ionic diffusion. We thus suggest that the different oxygen intake kinetics may be "intrinsic" and related to the different nature of the Al-O/Ga-O chemical bonds.

The transformation into the oxygen-excess form is confirmed by XRD patterns for the oxygenated products (Fig. S6 of the ESI). The patterns for the oxygenated $x = 0 \sim 0.5$ products are indexed assuming single-phase of the oxygen-excess-type structure,[32] despite the smaller excess oxygen amount than the ideal value. Crystallographic features of the "nonideal" oxygen-excess structure are still unclear and merits future investigations. Meanwhile, the pattern for the oxygenated $x = 1$ product is apparently a mixture of the oxygen-stoichiometric "$O_5$" and oxygen-excess "$O_{5.5}$" forms even after post-annealing for 20 h in flowing $O_2$ gas.

Next, temperature-induced oxygen intake/release characteristics were investigated employing TG up to 700 °C with heating/cooling rates of 2 °C/min. For $x = 0$ (Ga-free), the sample weight and accordingly the oxygen content increase and then show a plateau

at 450 ~ 640 °C, followed by an abrupt drop at 640 °C upon heating under $O_2$ atmosphere (Fig. 6). In the subsequent cooling scan, a large increase in the oxygen content appears at 610 °C without oxygen release upon further cooling. The oxygen intake/release behavior essentially agrees with that in our previous report.[6] While the $x$ = 0.1 product exhibits a similar behavior to $x$ = 0, its onset temperatures of oxygen release (upon heating) and oxygen re-intake (upon cooling) are slightly lowered. Furthermore, the lowering of the oxygen intake/release temperatures is remarkable for the Ga-rich products $x$ = 0.3 and 0.5, as summarized in Table 2. The oxygen intake/release rates of the fully Ga-substituted $x$ = 1 product were too sluggish to respond to the temperature variations, and we were unable to determine the onset temperatures with sufficient accuracy.

## 4. Discussion

The present work has demonstrated that the redox characteristics of $BaYMn_2O_{5+\delta}$ and $Ca_2AlMnO_{5+\delta}$ are greatly influenced by chemical substitutions at the cationic sites. Noticeably, both of these oxides contain layered cationic arrangements (Ba/Y for the former and Al/Mn for the latter), which lead to well-defined “active” sites for oxygen intake/release. It should be noted that the active oxygen neighbors the substituted cationic sites: that is, the yttrium site in $BaYMn_2O_{5+\delta}$ and aluminum site in $Ca_2AlMnO_{5+\delta}$, both of which are likely to play important roles in the oxygen intake/release processes through direct chemical bonds within the active oxygen layers. Such a common structural feature ensures the interpretation of the redox characteristics

variations in these oxides from similar points of view.

The Ba*Ln*$Mn_2O_{5+\delta}$ series is featured with its maximum range of oxygen-content variation up to $\delta \approx 1$, irrespective of the constituent $Ln^{3+}$ ion. It is hence practically impossible to discuss the *Ln* substitution effect focusing on the upper limit of oxygen contents. On the other hand, the isostructural cobalt oxides Ba*Ln*$Co_2O_{5+\delta}$ were found to crystallize in a partially oxygenated form even under oxygen-rich atmospheres showing a systematic trend of the highest $\delta$ value: $\delta \approx 0.7$ for larger *Ln* = Pr and Nd, $\delta \approx 0.4$ for moderate Sm, Eu, Gd, and Tb, and $\delta \approx 0.3$ for smaller Dy and Ho.[33] This finding is consistent with the results of our isothermal TG experiments on Ba*Ln*$Mn_2O_{5+\delta}$, where larger *Ln* members tend to show larger oxygen contents.

The *Ln*-dependent redox characteristics of Ba*Ln*$Mn_2O_{5+\delta}$ may be explained on the basis of coordination tendency of $Ln^{3+}$ ions. It is widely known that lanthanoid sesquioxides ($Ln_2O_3$) crystallize in three distinct types, which are characterized by coordination geometry of the so-called A-type (*Ln* = La ~ Nd), B-type (Sm ~ Dy), and C-type (Y), containing 7-coordinated, 7-/6-coordinated, and 6-coordinated *Ln* sites, respectively.[34] This implies that *Ln* species with larger ionic sizes preferably form larger coordination numbers (CN). Taking into account the fact that the oxygen intake process of Ba*Ln*$Mn_2O_{5+\delta}$ is directly linked to the increase in CN (from 8 to 10 ~ 12) at the *Ln* site, see Fig. 1(a), one can readily anticipate that the oxygenated forms are effectively stabilized especially for larger *Ln* members. The energetics of the oxygen intake/release processes was theoretically studied for *Ln* = Y employing quantum chemical calculations.[35] Similar calculations could be fruitful for other *Ln* members to see

whether the oxygen intake reaction is indeed more advantageous for larger *Ln* members.

Bearing in mind the similarity in the substitution strategy for Ba*Ln*$Mn_2O_{5+\delta}$ and $Ca_2Al_{1-x}Ga_xMnO_{5+\delta}$, the redox characteristics of the latter can also be discussed on the basis of the relative stability of the oxygenated forms, that is, the magnitude of energy gain upon oxygen intake. Our previous TG experiment indicated[6] that the oxygen intake/release behaviors at about 600 °C are accompanied by a first order phase transformation between low-*T* oxygen-excess ($\delta \approx 0.4$) and high-*T* oxygen-stoichiometric ($\delta \approx 0$) forms, implying that the transformation temperature corresponds to the upper limit of the oxygen-excess form as a thermodynamic stable phase. It is thus reasonable to assume that the transformation temperature should be lowered accordingly when the oxygen-excess form gets destabilized. In fact, the reported values of chemical bond strengths are $D° = 511 \pm 3$ for Al-O and $353.5 \pm 41.8$ kJ $mol^{-1}$ for Ga-O (at 298 K):[36] the much smaller value for the latter suggests the reducing stability of the oxygen-excess form and thereby the lowering transformation temperature upon Ga-for-Al substitution. We point out that the much slower oxygen-intake rate for the fully Ga-substituted product is also attributed to the less strong chemical bonds between Ga and excess oxygen atoms.

## 5. Conclusions

The present work demonstrated that the redox characteristics of two oxygen storage materials $BaYMn_2O_{5+\delta}$ and $Ca_2AlMnO_{5+\delta}$ can be controlled through isovalent

substitutions at the cationic sites; that is, lanthanoids (*Ln*) for yttrium and gallium for aluminum, respectively. While the redox species (= manganese) has remained untouched, the isovalent substitutions neighboring the active sites for oxygen intake/release are found to be very effective. Our finding thus provides a promising strategy of the materials design, that is, modifications of the local atomic environment around the active oxygen sites, to achieve "on-demand" redox characteristics. It is worth noting that the Ba*Ln*$Mn_2O_{5+\delta}$ product with the largest $La^{3+}$ ion can uptake oxygen even at 130 °C: this capability is advantageous for its practical application to reducing agent or oxygen removal (the use as an oxygen getter). Meanwhile, the lowered operating temperatures of Ga-substituted $Ca_2AlMnO_{5+\delta}$ could be favorable to realize the future application to oxygen-gas production/enrichment.

## Acknowledgements

The authors thank Dr. E. Tsuji of Hokkaido University for the SEM observations. The present work was supported by Grants-in-Aid for Science Research (Contract Nos. 22750181 and 26288104) from Japan Society for the Promotion of Science. T.M. acknowledges financial supports from Iketani Science and Technology Foundation.

## References

1. see, e.g., J. Kašpar and P. Fornasiero, *J. Solid State Chem.*, 2003, **171**, 19-29; J. Kašpar, P. Fornasiero and N. Hickey, *Catal. Today*, 2003, **77**, 419-449.
2. G. Dutta, U. V. Waghmare, T. Baidya, M. S. Hegde, K. R. Priolkar and P. R. Sarode, *Chem. Mater.*, 2006, **18**, 3249-3256.
3. N. Imanaka, T. Masui, K. Koyabu, K. Minami and T. Egawa, *Adv. Mater.*, 2007, **19**,

1608-1611.
4. M. S. Hegde, G. Madras and K. C. Patil, *Acc. Chem. Res.*, (2009), **42**, 704-712.
5. T. Motohashi, T. Ueda, Y. Masubuchi, M. Takiguchi, T. Setoyama, K. Oshima and S. Kikkawa, *Chem. Mater.*, 2010, **22**, 3192-3196.
6. T. Motohashi, Y. Hirano, Y. Masubuchi, K. Oshima, T. Setoyama and S. Kikkawa, *Chem. Mater.*, 2013, **25**, 372-377.
7. J. P. Chapman, J. P. Attfield, M. Molgg, C. M. Friend and T. P. Beales, *Angew. Chem. Int. Ed.*, 1996, **35**, 2482-2484.
8. F. Millange, E. Suard, V. Caignaert and B. Raveau, *Mater. Res. Bull.*, 1999, **34**, 1-9.
9. M. Karppinen, H. Okamoto, H. Fjellåg, T. Motohashi and H. Yamauchi, *J. Solid State Chem.*, 2004, **177**, 2122-2128.
10. K. Momma, F. Izumi, *J. Appl. Crystallogr.*, 2011, **44**, 1272-1276.
11. A. J. Wright, H. M. Palmer, P. A. Anderson and G. Greaves, *J. Mater. Chem.*, 2002, **12**, 978-982.
12. M. Zötzl and H. Pöllmann, *J. Am. Ceram. Soc.* 2006, **89**, 3491-3497.
13. E. V. Antipov, A. M. Abakumov and S. Y. Istomin, *Inorg. Chem.*, 2008, **47**, 8543-8552.
14. T. Nakajima, H. Kageyama, H. Yoshizawa and Y. Ueda, *J. Phys. Soc. Jpn.*, 2002, **71**, 2843-2846.
15. F. Millange, V. Caignaert, B. Domengès and B. Raveau, *Chem. Mater.*, 1998, **10**, 1974-1983.
16. S. V. Trukhanov, I. O. Troyanchuk, M. Hervieu, H. Szymczak and K. Bärner, *Phys. Rev. B*, 2002, **66**, 184424/1-84424/10.
17. E. Castillo-Martínez, A. J. Williams and J. P. Attfield, *J. Solid State Chem.*, 2006, **179**, 3505-3510.
18. R. Vidya, P. Ravindran, A. Kjekshus and H. Fjellvåg, *Phys. Rev. B*, 2007, **76**, 195114/1-195114/14.
19. K. Świerczek, A. Klimkowicz, K. Zheng and B. Dabrowski, *J. Solid State Chem.*, 2013, **203**, 68-73.
20. K. Świerczek, A. Klimkowicz, A. Niemczyk, A. Olszewska, T. Rząsa, J. Molenda and A. Takasaki, *Funct. Mater. Lett.*, 2014, 1440004.
21. A. Klimkowicz, K. Świerczek, K. Zheng, M. Baranowska, A. Takasaki and B. Dabrowski, *Solid State Ionics*, 2014, **262**, 659-663.
22. A. M. Abakumov, M. G. Rozova, B. Ph. Pavlyuk, M. V. Lobanov, E. V. Antipov, O. I. Lebedev, G. Van Tendeloo, D. V. Sheptyakov, A. M. Balagurov and F. Bourée, *J. Solid State Chem.*, 2001, **158**, 100-111.

23. A. M. Abakumov, M. G. Rozova, B. Ph. Pavlyuk, M. V. Lobanov, E. V. Antipov, O. I. Lebedev, G. Van Tendeloo, O. L. Ignatchik, E. A. Ovtchenkov, Yu. A. Koksharov and A. N. Vasil'ev, *J. Solid State Chem.*, 2001, **160**, 353-361.
24. A. M. Abakumov, A. S. Kalyuzhnaya, M. G. Rozova, E. V. Antipov, J. Hadermann and G. Van Tendeloo, *Solid State Sci.*, 2005, **7**, 801-811.
25. J. Hadermann, A. M. Abakumov, H. D'Hondt, A. S. Kalyuzhnaya, M. G. Rozova, M. M. Markina, M. G. Mikheev, N. Tristan, R. Klingeler, B. Büchner and E. V. Antipov, *J. Mater. Chem.*, 2007, **17**, 692-698.
26. V. Petricek, M. Dusek, and L. Palatinus, *Z. Kristallogr.* 2014, **229**, 345-352.
27. R. D. Shannon and C. T. Prewitt, *Acta Cryst.*, 1969, **B25**, 925-946.
28. T. Motohashi, T. Ueda, Y. Masubuchi and S. Kikkawa, *J. Ceram. Soc. Jpn.*, 2011, **119**, 894-897.
29. T. Motohashi, T. Takahashi, M. Kimura, Y. Masubuchi, S. Kikkawa, Y. Kubota, Y. Kobayashi, H. Kageyama, M. Takata, S. Kitagawa and Ryotaro Matsuda, *J. Phys. Chem. C*, 2015, **119**, 2356-2363.
30. C. Perca, L. Pinsard-Gaudart, A. Daoud-Aladine, M. T. Fernández-Díaz, J. Rodríguez-Carvajal, *Chem. Mater.*, 2005, **17**, 1835-1843.
31. A. A. Taskin, A. N. Lavrov and Y. Ando, *Appl. Phys. Lett.*, 2005, **86**, 091910/1-091910/3.
32. H. M. Parmer, A. Snedden, A. J. Wright and C. Greaves, *Chem. Mater.*, 2006, **18**, 1130-1133.
33. A. Maignan, C. Martin, D. Pelloquin, N. Nguyen and B. Raveau, *J. Solid State Chem.*, 1999, **142**, 247-260.
34. A. F. Wells, *Structural Inorganic Chemistry, Fifth Edition*, Oxford University Press Inc., New York, 1984.
35. M. Gilleßen, M. Lumeij, J. George, R. Stoffel, T. Motohashi, S. Kikkawa, R. Dronskowski, *Chem. Mater.*, 2012, **24**, 1910; *ibid* 2013, **25**, 4460.
36. W. M. Haynes (Ed.), *CRC Handbook of Chemistry and Physics, 95th Edition*, CRC Press/Taylor and Francis, Boca Raton, FL, 2014.

Table 1. Summary of data for the Ba*Ln*$Mn_2O_{5+\delta}$ series: tetragonal *a*- and *c*-axis lengths, excess oxygen content δ, and onset temperature of oxygen intake in flowing $O_2$ gas. The onset temperature is defined as the point for 5% weight gain. The values for ionic radii of $Ln^{3+}$ (CN = 8)[27] are also given.

| *Ln* | | Y | Gd | Nd | La* |
|---|---|---|---|---|---|
| ionic radius (CN = 8) / nm | | 0.1019 | 0.1053 | 0.1109 | 0.1160 |
| lattice parameters / nm | *a* | 0.55470(1) | 0.55772(1) | 0.56111(1) | 0.56498(1) |
| | *c* | 0.76515(1) | 0.76798(1) | 0.77334(1) | 0.78288(2) |
| excess oxygen content δ | | 0.006(6) | –0.01(2) | 0.05(2) | 0.01(2) |
| onset temperature (oxygen intake) / °C | | 250 | 225 | 160 | 130 |

*The sample was post-annealed at 500 °C in flowing 5% $H_2$/95% Ar gas mixture to completely remove excess oxygen.

Table 2. Summary of data for the $Ca_2Al_{1-x}Ga_xMnO_{5+\delta}$ series: orthorhombic *a*-, *b*-, and *c*-axis lengths, excess oxygen content δ, and onset temperatures of oxygen intake/release in flowing $O_2$ gas. The onset temperatures are defined as the points for 5% weight gain/loss.

| Ga content (*x*) | | 0 | 0.1 | 0.3 | 0.5 | 1.0 |
|---|---|---|---|---|---|---|
| lattice parameters / nm | *a* | 0.54657(1) | 0.54675(1) | 0.54684(1) | 0.54694(1) | 0.54671(1) |
| | *b* | 1.4992(0) | 1.5031(0) | 1.5093(0) | 1.5141(0) | 1.5302(0) |
| | *c* | 0.52398(1) | 0.52414(1) | 0.52468(1) | 0.52525(1) | 0.52635(1) |
| excess oxygen content δ | | 0.04(0) | 0.04(1) | 0.00(2) | 0.00(0) | –0.01(1) |
| onset temperature (oxygen intake) / °C | | 610 | 600 | 570 | 530 | – |
| onset temperature (oxygen release) / °C | | 640 | 630 | 600 | 550 | – |

## Figure captions

Fig. 1.
Schematic illustration of the crystal structures of (a) double-perovskite type $BaYMn_2O_{5+\delta}$ ($\delta$ = 0 and 1) and (b) Brownmillerite-type $Ca_2AlMnO_{5+\delta}$ ($\delta$ = 0 and 0.5). The illustration was drawn with VESTA software[10] based on the structural model reported in the literature.

Fig. 2.
TG curves of Ba*Ln*$Mn_2O_{5+\delta}$ with *Ln* = Y, Gd, Nd, and La. A portion of the as-synthesized product was heated in flowing $O_2$ gas from room temperature to 500 °C with a heating rate of 1 °C $min^{-1}$.

Fig. 3.
(a) Isothermal TG curve (700 °C) for $BaYMn_2O_{5+\delta}$ (*Ln* = Y) under decreased oxygen partial pressures from $P(O_2) = 10^5$ Pa to $10^2$ Pa. (b) Isothermal TG curve (700 °C) for $BaNdMn_2O_{5+\delta}$ (*Ln* = Nd) under decreased oxygen partial pressures from $P(O_2) = 10^5$ Pa to 10 Pa.

Fig. 4.
The $\delta$ vs. $P(O_2)$ plot for Ba*Ln*$Mn_2O_{5+\delta}$ with *Ln* = Y, Nd, and La based on the TG data: Fig. 3(a) for the Y-product between $P(O_2) = 10^5$ Pa and $10^2$ Pa, the data point at $P(O_2) = 10^1$ Pa was measured separately (not shown); Fig. 3(b) for the Nd-product; the TG curve for the La-product was also measured (not shown); plots of $BaGdMn_2O_{5+\delta}$ reported by Taskin and Ando[31] are also presented in this figure.

Fig. 5.
Isothermal TG curves for the $Ca_2Al_{1-x}Ga_xMnO_{5+\delta}$ products with $x$ = 0, 0.1, 0.3, 0.5 and 1.0. The data were measured at 400 °C after switching the gas flow from $N_2$ to $O_2$.

Fig. 6.
Representative TG curves for $Ca_2Al_{1-x}Ga_xMnO_{5+\delta}$ ($x$ = 0, 0.1, and 0.5) up to 700 °C. The data were measured in flowing $O_2$ gas with a scan rate of ± 2°C $min^{-1}$.

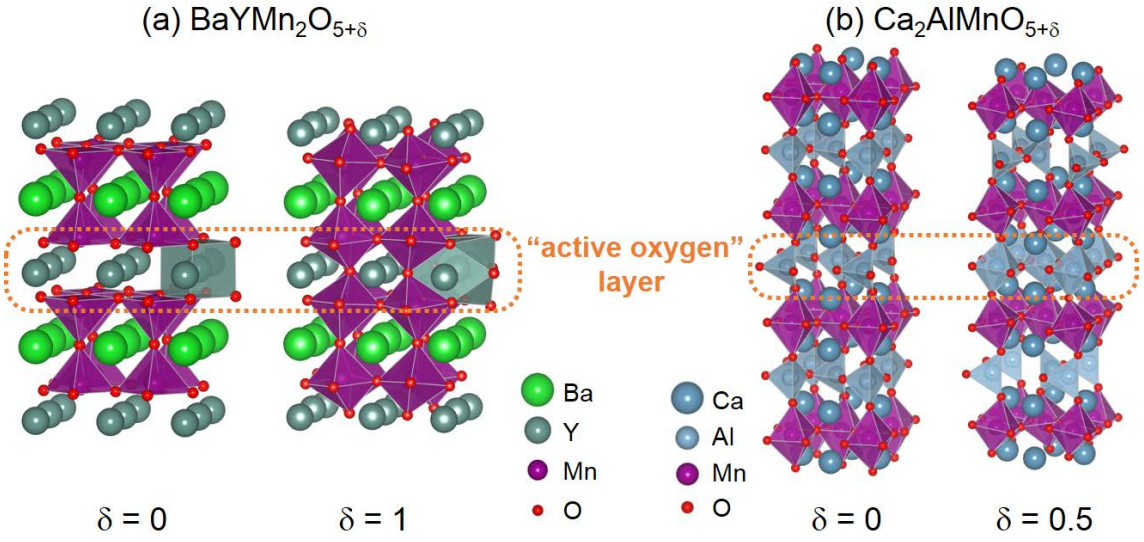


Fig. 1. Motohashi *et al.*

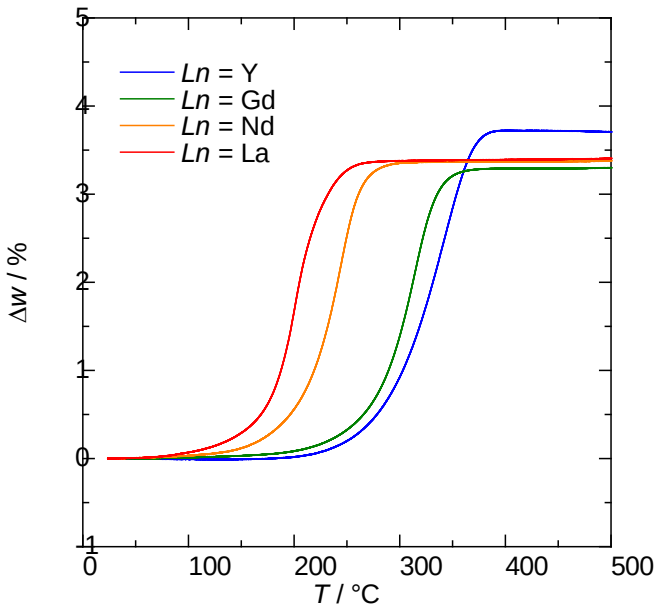


Fig. 2. Motohashi *et al.*

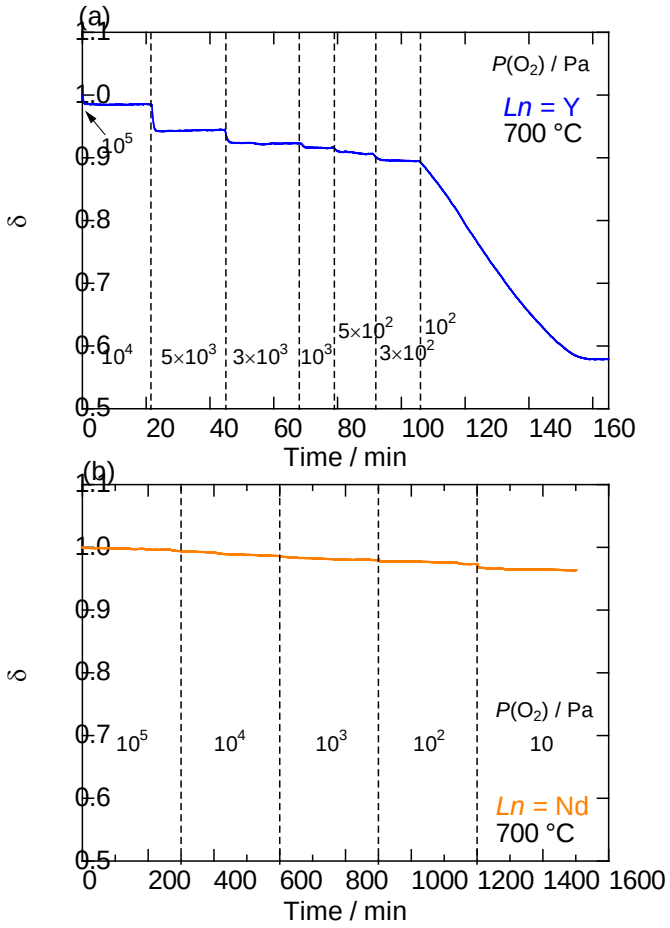


Fig. 3. Motohashi *et al.*

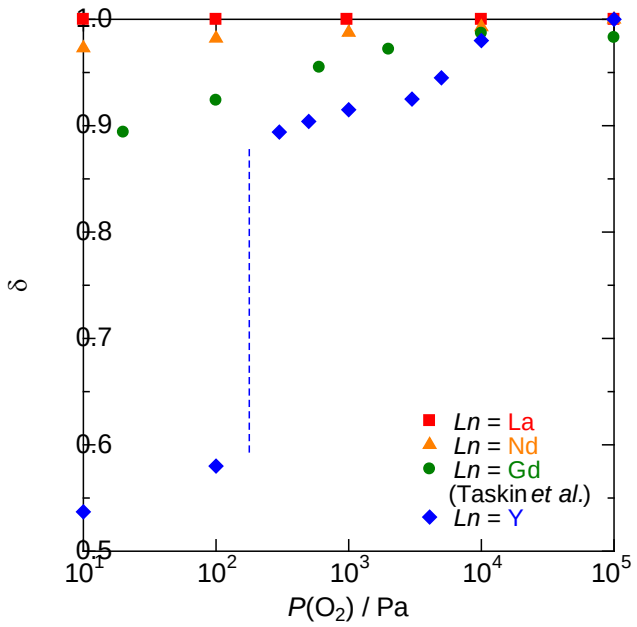


Fig. 4. Motohashi *et al.*

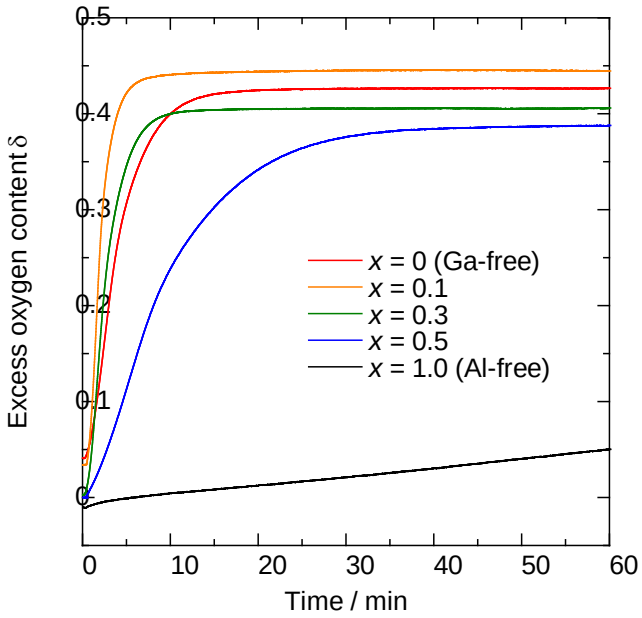


Fig. 5. Motohashi *et al.*

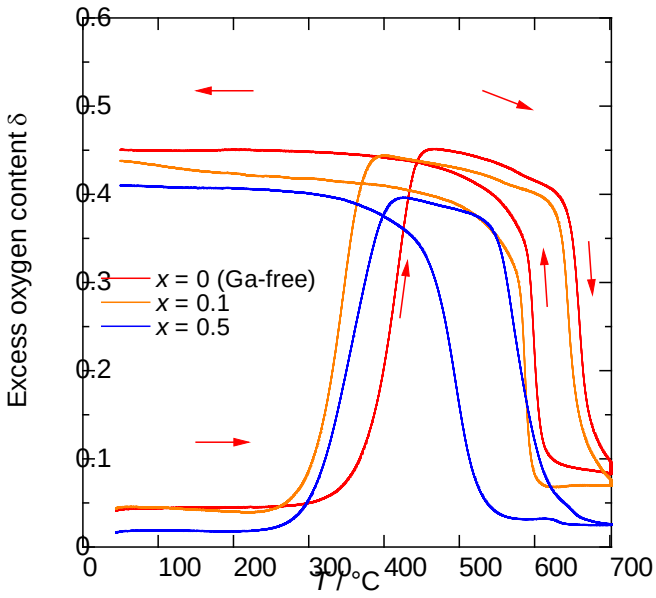


Fig. 6. Motohashi *et al.*